JOURNAL OF SPACECRAFT AND ROCKETS
Vol. 41, No. 6, November–December 2004

Engineering Notes

ENGINEERING NOTES are short manuscripts describing new developments or important results of a preliminary nature. These Notes cannot exceed six manuscript pages and three figures; a page of text may be substituted for a figure and vice versa. After informal review by the editors, they may be published within a few months of the date of receipt. Style requirements are the same as for regular contributions (*see inside back cover*).

Effect of Afterbody Configuration on Damping Coefficients for Axisymmetric Projectiles

Soo Hyung Park* and Jang Hyuk Kwon†
Korea Advanced Institute of Science and Technology, Daejeon 305-701, Republic of Korea

Nomenclature

C_m	=	pitching-moment coefficient
$C_{m_q} + C_{m_{\dot\alpha}}$	=	pitch-damping-moment coefficient (sum), $\frac{2U_\infty}{D}\frac{\partial C_m}{\partial \dot\alpha}$
$\tilde{C}_n$	=	side-moment coefficient in the body-fitted coordinate frame
D	=	reference length (base diameter), m
$\boldsymbol{F}$	=	inviscid flux vectors
$\boldsymbol{F}_v$	=	viscous flux vectors
$\boldsymbol{H}$	=	source vector
M	=	Mach number
p	=	spin rate, rad/s
$\boldsymbol{Q}$	=	conservative-flow-variable vector
q	=	pitch rate, rad/s
$\boldsymbol{S}_{k\omega}$	=	source vector of the k–ω equations
t	=	physical time, s
U_∞	=	freestream speed, m/s
$\boldsymbol{u}$	=	absolute velocity vector
α	=	angle of attack, deg
α_t	=	total angle of attack $\sqrt{(\alpha^2 + \beta^2)}$, deg
β	=	side-slip angle, deg
γ	=	$\cos\alpha_t$
δ	=	$\sin\alpha_t$
$\boldsymbol{\Omega}$	=	angular velocity vector

Superscript

$\cdot$	=	rate of change with respect to time

Introduction

STEADY coning motions in a noninertial rotating framework have been used commonly to predict pitch-damping coefficients.[1–3] The drawbacks of these methods are that they require the Magnus force or moment to be explicitly determined by other sources and that they sometimes require a geometrical constraint such as axisymmetry. Despite several deficiencies, the steady methods provide a cost-effective approach to the aerodynamics associated with unsteady or time-dependent motions.[4]

Previous steady methods have been based on the relationship between the pitch-damping coefficients and the side forces and moments due to coning motions. The methods used noninertial cylindrical formulations, which are appropriate in describing axisymmetric flows; therefore, the governing equations, with both complex source terms due to coordinate transformation and noninertial force terms, have been written in the cylindrical coordinate frame.[1,2]

The objectives of this study are to predict the damping coefficients of projectiles and to examine an effect of different afterbody configurations. It was argued in our previous work[3] that the steady coning motions used to predict the damping coefficient can be defined in the framework of the Cartesian coordinate frame. The noninertial formulation written in the Cartesian coordinate frame has been used to describe rotating flows with constant rotation rates, such as turbomachinery and rotor-blade flows.[5] The approach requires the noninertial force terms to be added only to the unsteady solver,[4] whereas a steady solution method is needed to predict the pitch-damping coefficients. The pitch-damping moment coefficients are predicted by using the zero-spin coning (combined spinning and coning) motion in the Cartesian coordinate frame. Using steady methods, the pitching and pitch-damping moments are computed and compared for the secant–ogive–cylinder (SOC) configurations.

Numerical Approach

Schiff[1] solved the steady Euler equations to compute the supersonic inviscid flow around the body during coning motions. The computation was based on the fact that the flow is steady if a rotating coordinate frame is used. He adopted a "lunar coning" motion to determine the pitch-damping coefficients from the side moments $\tilde{C}_n$. The formulation using the lunar coning motion represents a sum of the Magnus moment and the pitch-damping moment sum. To determine the pitch-damping moment sum directly, Weinacht et al.[2] proposed a "combined spinning and coning" motion that allows the side moment to be proportional to the pitch-damping moment only. For steady combined spinning and coning motion, the body rotates in the coning frame with a rate of rotation that is proportional to the coning rate Ω. Consequently, the spin rate of the body is zero, $p = 0$, and the side moment can be written as

$$\tilde{C}_n = \delta\left(\frac{\Omega D}{2U_\infty}\right)\left(C_{m_q} + \gamma C_{m_{\dot\alpha}}\right) \tag{1}$$

The detailed derivation of the relationship can be found in Refs. 1 and 2. Throughout this Note, this combined spinning and coning motion is referred to as zero-spin coning motion. In general, the rotation of the body relative to the coning frame will produce a time-dependent boundary condition and nonsteady flowfield. The zero-spin coning method is only a steady method for axisymmetric bodies, and requires a Navier–Stokes approach to implement the boundary condition correctly.[2]

The three-dimensional compressible full Navier–Stokes equations and variants of the k–ω turbulence equations[6–8] are considered

Presented as Paper 2004-0014 at the AIAA 42nd Aerospace Sciences Meeting, Reno, NV, 5–8 January 2004; received 6 February 2004; revision received 24 May 2004; accepted for publication 14 June 2004.

*Research Associate, Department of Aerospace Engineering; pish@kaist.ac.kr. Member AIAA.

†Professor, Department of Aerospace Engineering, 373-1 Guseong-dong, Yuseong-gu; jhkwon@kaist.ac.kr. Senior Member AIAA.

over the control volume $\mathcal{V}(t)$:

$$\frac{\mathrm{d}}{\mathrm{d}t}\int_{\mathcal{V}(t)} \boldsymbol{Q}\,\mathrm{d}\mathcal{V} + \int_{\partial\mathcal{V}(t)} (\boldsymbol{F}-\boldsymbol{F}_v)\,\mathrm{d}\mathcal{S} = \int_{\mathcal{V}(t)} (\boldsymbol{S}_{k\omega}+\boldsymbol{H})\,\mathrm{d}\mathcal{V} \quad (2)$$

The source term is defined as

$$\boldsymbol{H} = [0, \boldsymbol{h}\cdot\hat{\boldsymbol{i}}, \boldsymbol{h}\cdot\hat{\boldsymbol{j}}, \boldsymbol{h}\cdot\hat{\boldsymbol{k}}, \boldsymbol{h}\cdot\boldsymbol{u}, 0, 0]^T \quad (3)$$

$$\boldsymbol{h} = -\rho[\boldsymbol{\Omega}\times\boldsymbol{u}] \quad (4)$$

In this work, the following set of input data for the coning motion is specified:

$$\alpha = 2, \qquad \beta = 0, \qquad \boldsymbol{\Omega} = [\Omega_c\cos\alpha, 0, \Omega_c\sin\alpha]^T \quad (5)$$

To fulfill the conservation laws in the Cartesian coordinates, Eqs. (5) and resulting freestream conditions must be defined so that the following equation is satisfied at far field:

$$[\boldsymbol{\Omega}\times\boldsymbol{u}]_{r\to\infty} = 0 \quad (6)$$

The HLLE + scheme is used and the third-order MUSCL (monotone upstream scheme for conservation laws) interpolation method with the van Albada limiter is adopted to obtain second-order spatial accuracy.[9] The HLLE + scheme has been designed as an improvement in the family of Godunov-type schemes. It is more robust and accurate than the Roe scheme for supersonic viscous flows. Simple central differencing is applied to obtain the variable gradients of the viscous fluxes.

The diagonalized alternate directional implicit method is applied to find steady-state solutions for the Navier–Stokes and k–ω equations. A full approximate storage multigrid algorithm is used for convergence acceleration. The applied V-cycle multigrid algorithm concentrates on the acceleration of wave propagation rather than high-frequency damping. Finally, the code is parallelized for a cluster machine and two-layer cell-center values are transferred to the interface boundaries of each parallel block in order to retain the second-order accuracy near the interfaces. Each of the steady-state calculations required approximately 60–80 min of CPU time on a 24-Pentium 2.4-GHz LINUX cluster to converge the solution to 0.1% variation of the side-moment coefficient. The detailed numerical methods can be found in Ref. 3.

The side moments are obtained using zero-spin coning motions. It has been noted that the side-moment relations require linearity of the force and moment coefficients with $\Omega D/(2U_\infty)$ and $\sin\alpha$ (Ref. 2). The linearity is found in the present computations, though it is not displayed here. Computations are performed with coning rate $\Omega D/(2U_\infty) = 0.005$ and $\alpha = 2$ deg, which are enough to confirm the linearity.

Results and Discussion

Computations are performed to predict the static and dynamic stability coefficients for SOC configurations in the transonic and supersonic regimes. A schematic of the SOC-BoatTail (SOCBT), SOC, and SOC-Flare (SOCF) configurations is displayed in Fig. 1. The center of gravity is located at 60% of body length from the nose, and the Reynolds number is 4.5×10^6 based on the cylinder diameter. The main grid has 161 node points in the flow direction and 65

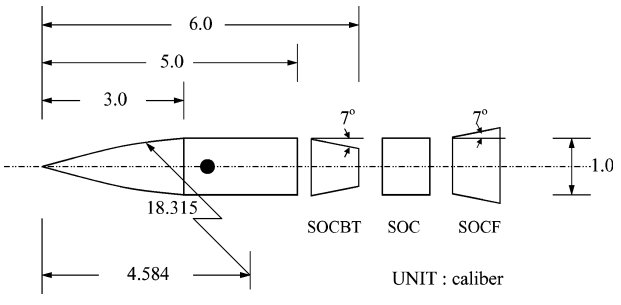

Fig. 1 SOCBT, SOC, and SOCF configurations.

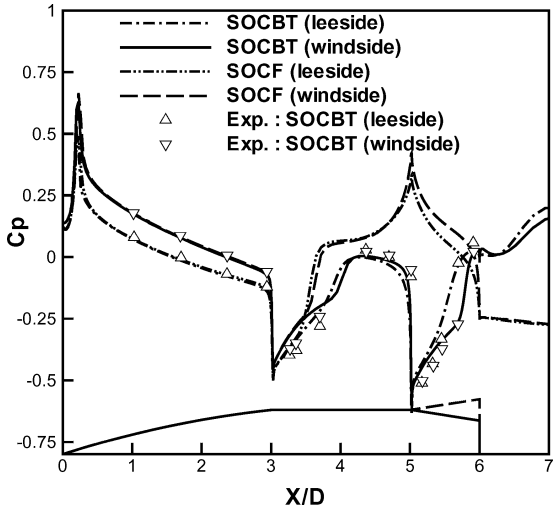

Fig. 2 Comparison of surface C_p distributions at $M = 0.96$ and $\alpha = 4$ deg.

and 97 points in the circumferential and radial directions, respectively. The base grid from the center of the body base to the farfield consists of 97 points in the flow direction and 65 and 129 points in the circumferential and radial directions. Previously, a grid convergence study was performed for the Army–Navy spinner rocket geometry using the same flow solver.[3] The differences between the present grids and finer grids are less than 2% for the pitch-damping coefficients.

Several researchers have predicted the static aerodynamic coefficients for the SOCBT configuration.[10] The pitch-damping characteristics for the SOC and SOCBT configurations have also been predicted using the parabolized Navier–Stokes equations and the steady coning motions.[2] A comparative study showed that the effect of the boattail in the supersonic regime is the reduction of the pitch-damping moment by 20–30% compared with that for the cylindrical afterbody. Furthermore, semiempirical predictions of pitch damping were made for configurations with flares and compared with the experimental and the computational data.[11]

Figure 2 displays the surface-pressure-coefficient distributions for the wind and lee sides of the SOCBT and SOCF configurations at $M = 0.96$. The agreement of the turbulent solution with experimental data[12] is good for both sides of the SOCBT configuration. Indeed, the difference between the laminar and the present turbulent results is marginal over the ogive and cylinder, whereas the discrepancy between the laminar results and the experimental data on the boattail is noticeable and makes a difference in the resulting pitching moment, shown in Fig. 3, at the transonic region. The expansions and recompressions near the ogive–cylinder and cylinder–boattail have been captured, whereas the flow over the SOCF configuration is compressed before the flare and expanded on the flare. Our research will show that this adverse effect of the flare against the boattail makes projectiles more stable statically and dynamically.

The development of the pitching moment integrated from the nose in Fig. 3 shows that the transonic critical behavior[10] in the slope of the pitching moment results from the variation of the pitching moment in the boattail. A discrepancy between the laminar and turbulent solutions is found near the boattail at $M = 0.98$, whereas variants of k–ω turbulence models[6–8] give nearly the same results (not shown). This implies that the turbulent flows over the configurations are nearly attached, because they produce similar solutions for the nearly attached flows.[8] The adverse effect of the flare is observed in Fig. 3. The pitching moment on the flare decreases as X/D increases, and it should be noted that the variations of the pitching moment with the Mach number over the nose and the cylindrical bodies are small for both configurations.

Figure 4 shows the variations of the pitch-damping moment coefficients with the Mach number for three configurations. The

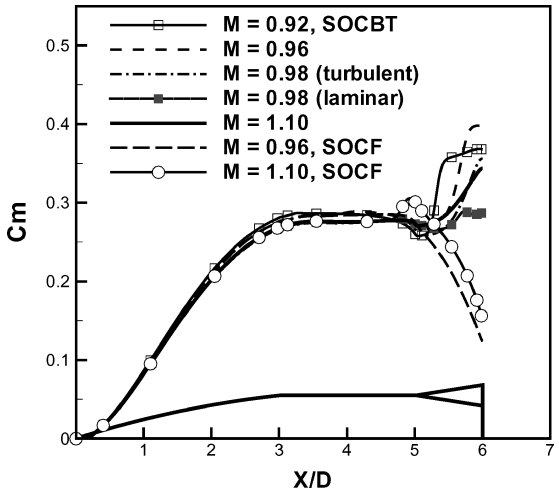

Fig. 3 Development of pitching-moment coefficient over SOCBT and SOCF configurations at $\alpha = 4$ deg.

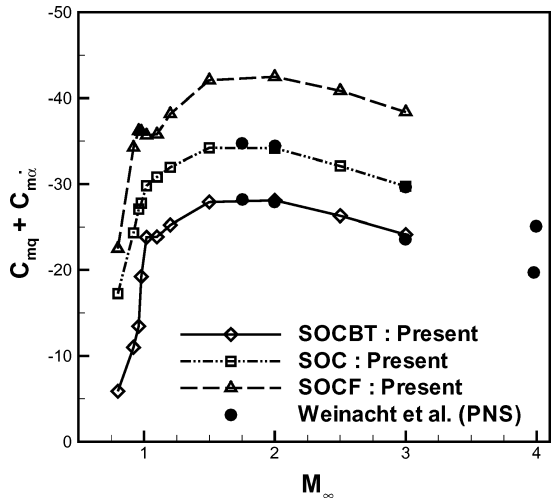

Fig. 4 Variation of pitch-damping-moment coefficient with Mach number for SOC, SOCBT, and SOCF configurations.

pitch-damping moment coefficients are in good agreement with the parabolized Navier–Stokes results,[2] and the pitch-damping moment coefficient has a decreasing trend up to $M = 2.0$. The variation with configuration in magnitude of the pitch-damping coefficient at the transonic region is higher than that at the supersonic region. The results also show that the presence of the boattail reduces the pitch damping compared with that for the cylindrical afterbody.

To elucidate the cause of the pronounced difference in magnitude, the developments of the pitch-damping moment coefficients over the bodies shown in Figs. 5 and 6 with Mach number are examined. The figures clearly illustrate the effect of the afterbody on the pitch-damping moments. The largest contribution to the pitch-damping moment is produced at the rear of the body, and it should be noted that the longitudinal variations are fairly consistent from highly subsonic to supersonic speeds. The variations for the SOCBT configuration at the supersonic region show behavior similar to that of those for the SOC and the SOCF configurations. On the other hand, the developments show transitional behavior from subsonic to supersonic speeds. A loss of pitch damping over the boattail is a result of the asymmetric distributions of the recompression fields on the boattail, but the expansion fields on the flare help developing the pitch-damping moment and improving overall stability characteristics.

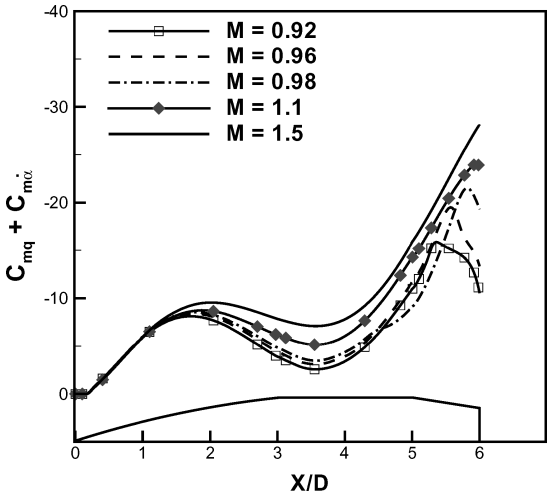

Fig. 5 Development of pitch-damping-moment coefficient over SOCBT configuration.

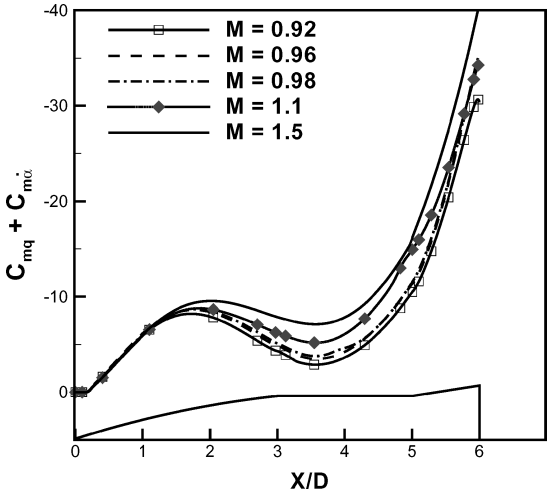

Fig. 6 Development of pitch-damping-moment coefficient over SOCF configuration.

Conclusions

A prediction method for the pitch-damping coefficients was presented in the unified framework of the turbulent Navier–Stokes equations. Using the relative velocities of the coning motions in the unsteady governing equations enables the prediction of the pitch-damping coefficients in a simple manner. The present methods were applied to predict the static aerodynamic coefficients and the pitch-damping coefficients for the SOC configurations with different afterbody configurations. The predictions showed that the flowfields due to the afterbody geometries significantly affect the pitching and pitch-damping moments.

References

[1]Schiff, L. B., "Nonlinear Aerodynamics of Bodies in Coning Motion," *AIAA Journal*, Vol. 10, No. 11, 1972, pp. 1517–1522.

[2]Weinacht, P., Sturek, W. B., and Schiff, L. B., "Navier–Stokes Predictions of Pitch Damping for Axisymmetric Projectiles," *Journal of Spacecraft and Rockets*, Vol. 34, No. 6, 1997, pp. 753–761.

[3]Park, S. H., and Kwon, J. H., "Navier–Stokes Computation of Pitch–Damping Coefficients Using Steady Coning Motions," *Journal of Spacecraft and Rockets*, Vol. 41, No. 5, 2004, pp. 754–761.

[4]Park, S. H., Kim, Y., and Kwon, J. H., "Prediction of Damping Coefficients Using the Unsteady Euler Equations," *Journal of Spacecraft and Rockets*, Vol. 40, No. 3, 2003, pp. 356–362.

[5]Chen, J. P., Ghosh, A. R., Sreenivas, K., and Whitfield, D. L., "Comparison of Computations Using Navier–Stokes Equations in Rotating and Fixed Coordinates for Flow Through Turbomachinery," AIAA Paper 97-0878, Jan. 1997.

[6]Wilcox, D. C., "Reassessment of the Scale-Determining Equation for Advanced Turbulence Models," *AIAA Journal*, Vol. 26, No. 11, 1988, pp. 1299–1310.

[7]Menter, F. R., "Two-Equation Eddy-Viscosity Turbulence Models for Engineering Applications," *AIAA Journal*, Vol. 32, No. 8, 1994, pp. 1598–1605.

[8]Park, S. H., and Kwon, J. H., "Implementation of k–ω Turbulence Models in an Implicit Multigrid Method," *AIAA Journal*, Vol. 42, No. 7, 2004, pp. 1348–1357.

[9]Park, S. H., and Kwon, J. H., "On the Dissipation Mechanism of Godunov-Type Schemes," *Journal of Computational Physics*, Vol. 188, No. 2, 2003, pp. 524–542.

[10]Sahu, J., "Numerical Computations of Transonic Critical Aerodynamic Behavior," *AIAA Journal*, Vol. 28, No. 5, 1990, pp. 807–816.

[11]Moore, F. G., and Hymer, T. C., "Semiempirical Prediction of Pitch Damping Moments for Configurations with Flares," *Journal of Spacecraft and Rockets*, Vol. 38, No. 2, 2001, pp. 150–158.

[12]Kayser, L. D., and Whiton, F., "Surface Pressure Measurements on a Boattailed Projectile Shape at Transonic Speeds," U.S. Army Ballistic Research Lab., Rept. AR-BRL-MR-03161, Aberdeen Proving Ground, MD, March 1982.

R. Cummings
Associate Editor